Steel and Composite Structures, *Vol. 36, No. 1* (*2020*) *87-101*
DOI: https://doi.org/10.12989/scs.2020.36.1.087

Investigating nonlinear forced vibration behavior of multi-phase nanocomposite annular sector plates using Jacobi elliptic functions

Seyed Sajad Mirjavadi[1], Masoud Forsat*[2], Mohammad Reza Barati[3] and A.M.S. Hamouda[1]

[1]*Department of Mechanical and Industrial Engineering, Qatar University, P.O. Box 2713, Doha, Qatar*
[2]*Department of Civil and Architectural Engineering, Qatar University, Doha, Qatar*
[3]*Fidar project Qaem Company, Darvazeh Dolat, Tehran, Iran*

(*Received February 25, 2020, Revised May 19, 2020, Accepted May 21, 2020*)

Abstract. A multi-scale epoxy/CNT/fiberglass annular sector plate is studied in this paper in the view of determining nonlinear forced vibration characteristics. A 3D Mori-Tanaka model is employed for evaluating multi-scale material properties. Thus, all of glass fibers are assumed to have uni-direction alignment and CNTs have random diffusion. The geometry of annular sector plate can be described based on the open angle and the value of inner/outer radius. In order to solve governing equations and derive exact forced vibration curves for the multi-scale annular sector, Jacobi elliptic functions are used. Obtained results demonstrate the significance of CNT distribution, geometric nonlinearity, applied force, fiberglass volume, open angle and fiber directions on forced vibration characteristics of multi-scale annular sector plates.

Keywords: forced vibration; annular sector; annular plate; nano-composite material; multi-scale composite

1. Introduction

Scientists are persistently working to accomplish more comfortable life for human and to establish modern applied sciences. Thus, the requirement for smart and advanced materials has grown, and existent technologies are frequently exchanged by progressive technologies (Feng *et al.* 2017, Zhang *et al.* 2017, Dong *et al.* 2018, Safaei *et al.* 2019, Mirjavadi *et al.* 2017, 2018, 2019, Azimi *et al.* 2017, 2018). A polymeric material has already replaced ordinary materials including metals and ceramics because of its low weight, easy manufacturing, and low costs (Thanh *et al.* 2019, Ahmed *et al.* 2019). Therewith, a polymer possesses prominent corrosion stability and promising mechanical character. But, there are some disadvantages related to polymeric components, including slight thermal stability, downscale stiffness and environmental stability. In order to eschew such sorts of disadvantages, polymeric composites were manufactured via reinforcement of matrices based on an extensive range of filler materials (Vo *et al.* 2017, Houari *et al.* 2018). According to the desirable performances of the conclusive material, the polymeric matrix may be reinforced via different kinds of macro to nano size fillers including fibers, particles and even platelets (Wu *et al.* 2017, Zhao *et al.* 2017). The performances of produced composite rely on the properties of both host material and filler. However, the performances of polymeric materials will decrease by passing time because of diverse factors including subjecting to UV, high temperatures or moisture. Composites which contain polymeric matrix and fiber reinforcement are produced to prevail such problems and enhance the overall performances of composite materials.

Fibers in reinforced polymeric materials represent remarkable characteristics including desired flexibility, aspect ratio and stability while the matrix defends the fibers against unfair conditions and retains their location. Nowadays, diverse sorts of artificial and synthetic fibers have been employed for reinforcing the polymeric matrices and then improving the performances of the final product. Such reinforced composites are applied in a variety of engineering fields such as aerospace, ocean and even automobiles, owning to the their desired cost and weight together with notable strength. For improving the out-of-plane performances of a composite, more than one filler element is needed. Note that weight is a very vital parameter in several applications including space vehicles and automobiles, and large size fillers yield higher to weights. Accordingly, nano scale fillers are often prior to macro scale counterparts. Multiple investigations have proved the elevated mechanical, thermal, and electrical characteristics of a nanoparticle reinforced composite. An advanced composite made from embedded fibers and reinforcing nano-dimension fillers (graphene, carbon nanotube, ant etc.) is introduced as a multi-scale composite (Marynowski 2017, Wattanasakulpong and Chaikittiratana 2015, Barati and Zenkour 2017). Such kind of composite is also defined as a multi-function composite due to possessing conventional load-sharing character of fiber reinforced material and also the extra functional characteristics (stiffness, strength, conductivity) related to the specific nanomaterials. Also, there are some researches on multi-phase composites with piezo-magnetic constituents (Mahesh *et al.* 2018, 2019, Mahesh and Kattimani 2019, Vinyas and Kattimani2017, 2018, Vinyas *et al.* 2019,2020, Vinyas 2020, Ebrahimi *et al.* 2019).

∗Corresponding author, Ph.D.
E-mail: masoudforsatlar@gmail.com

ISSN: 1229-9367 (Print), 1598-6233 (Online)

According to recent studies, the multi-scale composite can be modeled via several approaches including Halpin-Tsai and Eshelby-Mori-Tanaka forms (Mori and Tanaka 1973). Although the Eshelby–Mori–Tanaka approach has high efficacy for multi-scale material modeling, it sometimes yields an asymmetric stiffness tensor for the composites, whereas, the 3D Mori-Tanaka's stiffness tensor, is always symmetric (Kazakov *et al.* 2019). The later can be used as an efficient tool for elastic properties definition of multi-scale composite. Also, there are many publications on vibration analysis of multi-scale composite structures, there is no investigation on nonlinear vibrations of annular sectors made of hybrid epoxy/fiberglass/CNT material.

It must be stated that annular plates possess remarkable applications in diverse engineering sections including defense industry, semi-conductors, space vehicle, chemical plants and bio-medical sectors. Recently, few studies are devoted to examine mechanical characteristics of annular plates made of composite materials. Dai *et al.* (2019) examined vibrational behavior of annular plates reinforced by functional gradation of nanotubes in hygro-thermal environments. An investigation on vibrations of graphene reinforced annular plates is performed by Liu *et al.* (2019). Also, Keleshteri *et al.* (2019) studied nonlinear bending behavior of carbon nanotube reinforced annular plates with variable thickness. Safarpour *et al.* (2020) researched linear vibrations of graphene reinforced annular plates based on a numerical approach. Based on a higher order theory, Wang *et al.* (2020) researched free vibrations of graphene reinforced annular plates under thermal load. According to the best of our knowledge, nonlinear forced vibrations of multi-scale epoxy/CNT/fiberglass annular sector plates under external harmonic loads is not studied before.

Studied in this paper is nonlinear forced vibration behavior of a multi-scale epoxy/CNT/fiberglass annular sector plate subjected to transverse harmonic load and rested on elastic foundation. A 3D Mori-Tanaka model is employed for evaluating multi-scale material properties. Therefore, all of glass fibers are assumed to have uni-direction alignment and CNTs have random diffusion. The geometry of annular sector plate can be described based on the open angle and the value of inner/outer radius. In order to solve governing equations and derive exact forced vibration curves for the multi-scale annular sector, Jacobi elliptic functions are used. Obtained results demonstrate the significance of CNT distribution, geometric nonlinearity, applied force, fiberglass volume, open angle and fiber directions on forced vibration characteristics of multi-scale annular sector plates. In this paper, classic plate/shell theory has been used. However, there are many papers based on higher order theories (Abualnour *et al.* 2019, Addou *et al.* 2019, Balubaid *et al.* 2019, Berghouti *et al.* 2019, Bouamoud *et al.* 2019, Boulefrakh *et al.* 2019, Draiche *et al.* 2019, Draoui *et al.* 2019, Hellal *et al.* 2019, Hussain *et al.* 2019, Kaddari *et al.* 2020, Karami *et al.* 2019, Khiloun *et al.* 2019, Khosravi *et al.* 2020, Mahmoudi *et al.* 2019, Medani *et al.* 2019, Meksi *et al.* 2019, Refrafi *et al.* 2020, Rahmani *et al.* 2020, Sahla *et al.* 2019, Semmah *et al.* 2019, Soltani *et al.* 2019, Tlidji *et al.* 2019, Tounsi *et al.* 2020, Zarga *et al.* 2019, Zaoui *et al.* 2019).

2. Properties of multi-scale CNT/fiberglass/epoxy composite

In this research, a 3D Mori-Tanaka model is employed for evaluating multi-scale material properties. Also, all of glass fibers are assumed to have uni-directional alignment and CNTs have random diffusion (Fig. 1). The first issue is calculating material properties of a nano-composite (epoxy+ CNTs) which are elastic moduli (E_{11}, E_{22}), shear moduli (G_{12}, G_{23}) and bulk modulus (K_{23}) as (Kazakov *et al.* 2019)

$$\frac{E_{11}}{E_m}=\frac{1}{1+V_{cnt}\left(A_1+2\mu_m A_2\right)/\tilde{A}} \tag{1}$$

$$\frac{E_{22}}{E_m}=\frac{1}{1+V_{cnt}\left(\left(1-\mu_m\right)A_4-2\mu_m A_3+\left(1+\mu_m\right)A_5\tilde{A}\right)/2\tilde{A}} \tag{2}$$

$$G_{12}=G_m+\frac{G_m V_{cnt}}{\frac{G_m}{\Delta G}+2\left(1-V_{cnt}\right)S_{1212}} \tag{3}$$

$$G_{23}=G_m+\frac{G_m V_{cnt}}{\frac{G_m}{\Delta G}+2\left(1-V_{cnt}\right)S_{2323}} \tag{4}$$

$$K_{23}=\frac{\left(G_m+\lambda_m\right)\left(1+\mu_m\right)\left(1-2\mu_m\right)}{1-\mu_m\left(1+2\mu_{12}\right)+\frac{V_{cnt}}{\tilde{A}}\left(2\left(\mu_{12}-\mu_m\right)A_3+\left(1-\mu_m\left(1+2\mu_{12}\right)\right)A_4\right)} \tag{5}$$

in which $\Delta G=G_{cnt}-G_m$; G_{cnt} and G_m denote nanotube and matrix shear modulus, respectively. In addition, E_m and μ_m denote Young's modulus and Poisson ratio of matrix material; V_{cnt} defines CNT volume fraction which is associated with CNTs weight fraction (W_{cnt}), matrix density (ρ_m) and CNT density (ρ_{cnt}) as

$$V_{cnt}=\frac{W_{cnt}\rho_m}{\left(1-W_{cnt}\right)\rho_{cnt}+W_{cnt}\rho_m} \tag{6}$$

Moreover, the parameters A_i (i=1, 2, 3, 4, 5) should be determined by

$$\begin{aligned}
&A_1=D_1\left(B_4+B_5\right)-2B_2,\\
&A_2=\left(1+D_1\right)B_2-\left(B_4+B_5\right),\\
&A_3=B_1-D_1B_3,\\
&A_4=\left(1+D_1\right)B_1-2B_3,\\
&A_5=\frac{1-D_1}{B_4-B_5},\\
&\tilde{A}=2B_2B_3-B_1\left(B_4+B_5\right)
\end{aligned} \tag{7}$$

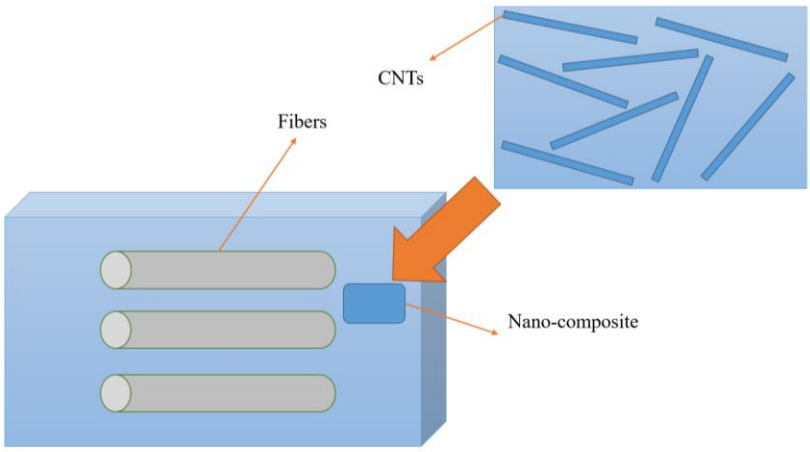

Fig. 1 A multi-scale composite element reinforced with fibers and CNTs

Next, the parameters in above relations may be defined as

$$\begin{aligned}
B_1 &= V_{cnt}D_1 + D_2 + (1-V_{cnt})(D_1S_{1111} + 2S_{2211}),\\
B_2 &= V_{cnt} + D_3 + (1-V_{cnt})(D_1S_{1122} + S_{2222} + S_{2233}),\\
B_3 &= V_{cnt} + D_3 + (1-V_{cnt})(S_{1111} + (1+D_1)S_{2211}),\\
B_4 &= V_{cnt}D_1 + D_2 + (1-V_{cnt})(S_{1122} + D_1S_{2222} + S_{2233}),\\
B_5 &= V_{cnt} + D_3 + (1-V_{cnt})(S_{1122} + S_{2222} + D_1S_{2233})
\end{aligned} \tag{8}$$

in which S_{ijkl} denote the components of Eshelby's tensor which are introduced in the Appendix and

$$\begin{aligned}
D_1 &= 1 + 2\frac{G_{cnt} - G_m}{\lambda_{cnt} - \lambda_m},\\
D_2 &= \frac{\lambda_m + 2G_m}{\lambda_{cnt} - \lambda_m},\\
D_3 &= \frac{\lambda_m}{\lambda_{cnt} - \lambda_m}
\end{aligned} \tag{9}$$

It must be stated that λ_m and λ_{cnt} define Lame's constants of matrix and CNT, respectively determined by

$$\begin{aligned}
\lambda_m &= \frac{\mu_m E_m}{(1-2\mu_m)(1+\mu_m)},\\
\lambda_{cnt} &= \frac{\mu_{cnt} E_{cnt}}{(1-2\mu_{cnt})(1+\mu_{cnt})}
\end{aligned} \tag{10}$$

Next, it must be stated that the nano-composite material has below definitions for the bulk modulus $\hat{K}$ and shear modulus $\hat{G}$ as

$$\hat{K} = \frac{E_{11} + 4(1+\mu_{12})^2 K_{23}}{9} \tag{11}$$

$$\hat{G} = \frac{E_{11} + (1-2\mu_{12})^2 K_{23} + 6(G_{12} + G_{23})}{15} \tag{12}$$

Table 1 Material properties of hybrid multi-scale composite material (Kazakove *et al.* 2019)

Material property	Value
Young modulus of matrix (E_m)	3.45 GPa
Young modulus of CNTs (E_{cnt})	1 TPa
Young modulus of fiberglass (E_f)	73.1 GPa
Density of matrix (ρ_m)	1270 kg/m^3
Density of CNTs (ρ_{cnt})	110 kg/m^3
Poisson's ratio of the matrix (μ_m)	0.35
Poisson's ratio of the CNTs (μ_{cnt})	0.17
Poisson's ratio of the fiberglass (μ_f)	0.22

In the case of multi-scale materials, the nano-composite part is defined as host material (matrix) and the glass fibers are macro scale fillers. Therefore, Young's modulus $\hat{E}$ and Poisson ratio $\hat{\mu}$ of host material are defined as

$$\hat{E} = \frac{9\hat{G}\hat{K}}{3\hat{K} + \hat{G}},\ \hat{\mu} = \frac{\hat{E}}{2\hat{G}} - 1 \tag{13}$$

For incorporating the effect of glass fiber as infinite filler with $\alpha \to \infty$, Eqs. (1)-(5) may be employed again. However, these equations should be modified by considering fiber volume fraction (V_f) instead of V_{cnt} and also all properties related to nano-composite material should be considered as the properties of matrix material. All properties of the ingradients are presented in Table 1.

3. Formulation for annular sector plates

Considering inner radius (r_0), outer radius (r_1) and open angel (ψ), Fig. 2 illustrates the geometry of an annular sector plate. Also, an annular sector subjected to transverse uniform harmonic load is shown in Fig. 3. For a thin annular sector plate, components of strain field are (Barati and Zenkour 2019)

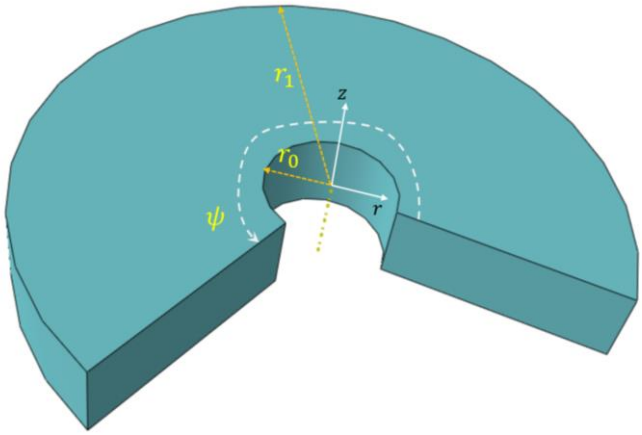

Fig. 2 Geometry of the annular sector plate

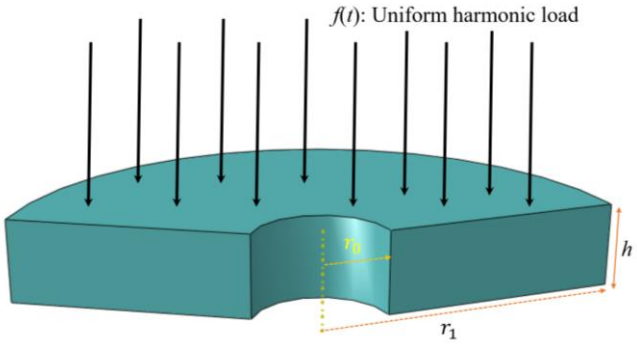

Fig. 3 An annular sector plate exposed to external harmonic load

$$\begin{aligned}\varepsilon_r &= \varepsilon_r^0 - z\chi_r,\\ \varepsilon_\varphi &= \varepsilon_\varphi^0 - z\chi_\varphi,\\ \gamma_{r\varphi} &= \gamma_{r\varphi}^0 - 2z\chi_{r\varphi}.\end{aligned} \tag{14}$$

in which

$$\begin{aligned}\varepsilon_r^0 &= \frac{\partial u}{\partial r} + \frac{1}{2}\left(\frac{\partial w}{\partial r}\right)^2,\\ \varepsilon_\varphi^0 &= \frac{1}{r}\left(\frac{\partial v}{\partial \varphi} + u\right) + \frac{1}{2r^2}\left(\frac{\partial w}{\partial \varphi}\right)^2,\\ \gamma_{r\varphi}^0 &= \frac{1}{r}\frac{\partial u}{\partial \varphi} + \frac{\partial v}{\partial r} - \frac{v}{r} + \frac{1}{r}\frac{\partial w}{\partial r}\frac{\partial w}{\partial \varphi},\\ \chi_r &= \frac{\partial^2 w}{\partial r^2},\ \ \chi_\varphi = \frac{1}{r}\frac{\partial w}{\partial r} + \frac{1}{r^2}\frac{\partial^2 w}{\partial \varphi^2},\\ \chi_{r\varphi} &= \frac{1}{r}\frac{\partial^2 w}{\partial r \partial \varphi} - \frac{1}{r^2}\frac{\partial w}{\partial \varphi}\end{aligned} \tag{15}$$

Sector deflection is denoted by w and in-plane displacements are denoted by u and v. As mentioned, the annular sector is made of fiber-reinforced multi-scale material for which the stresses σ_p (p=r, φ, $r\varphi$) can be determined as

$$\begin{Bmatrix}\sigma_r\\ \sigma_\varphi\\ \sigma_{r\varphi}\end{Bmatrix} = \begin{pmatrix}\tilde{Q}_{11} & \tilde{Q}_{12} & \tilde{Q}_{16}\\ \tilde{Q}_{12} & \tilde{Q}_{22} & \tilde{Q}_{26}\\ \tilde{Q}_{16} & \tilde{Q}_{26} & \tilde{Q}_{66}\end{pmatrix}\begin{Bmatrix}\varepsilon_r\\ \varepsilon_\varphi\\ \gamma_{r\varphi}\end{Bmatrix} \tag{16}$$

in which Q_{ij} may be introduced by

$$\begin{aligned}&\tilde{Q}_{11} = Q_{11}(\cos\theta)^4\\ &+2(Q_{12}+2Q_{66})(\sin\theta)^2(\cos\theta)^2\\ &+Q_{22}(\sin\theta)^4,\\ &\tilde{Q}_{12} = (Q_{11}+Q_{22}-4Q_{66})(\sin\theta)^2(\cos\theta)^2\\ &+Q_{12}\left((\sin\theta)^4+(\cos\theta)^4\right),\\ &\tilde{Q}_{16} = (Q_{11}-Q_{12}-2Q_{66})(\sin\theta)(\cos\theta)^3\\ &+(Q_{12}-Q_{22}+2Q_{66})(\sin\theta)^3(\cos\theta),\\ &\tilde{Q}_{22} = Q_{11}(\sin\theta)^4\\ &+2(Q_{12}+2Q_{66})(\sin\theta)^2(\cos\theta)^2\\ &+Q_{22}(\cos\theta)^4,\\ &\tilde{Q}_{26} = (Q_{11}-Q_{12}-2Q_{66})(\sin\theta)^3(\cos\theta)\\ &+(Q_{12}-Q_{22}+2Q_{66})(\sin\theta)(\cos\theta)^3,\\ &\tilde{Q}_{66} = \begin{pmatrix}Q_{11}+Q_{22}-2Q_{12}\\ -2Q_{66}\end{pmatrix}(\sin\theta)^2(\cos\theta)^2\\ &+Q_{66}\left((\sin\theta)^4+(\cos\theta)^4\right).\end{aligned} \tag{17}$$

where θ denotes orientation of fibers about r-axis and

$$Q_{11}=\frac{E_{11}}{1-\mu_{12}\mu_{21}},\quad Q_{12}=\frac{\mu_{12}E_{22}}{1-\mu_{12}\mu_{21}},\quad Q_{22}=\frac{E_{22}}{1-\mu_{12}\mu_{21}},\quad Q_{66}=G_{12} \tag{18}$$

Annular sector plate contains stresses which result in below forces and moments via integrating Eq. (16) over sector thickness

$$\begin{Bmatrix}N_r\\N_\varphi\\N_{r\varphi}\end{Bmatrix}=\begin{pmatrix}A_{11}&A_{12}&A_{16}\\A_{12}&A_{22}&A_{26}\\A_{16}&A_{26}&A_{66}\end{pmatrix}\begin{Bmatrix}\varepsilon_r^0\\\varepsilon_\varphi^0\\\gamma_{r\varphi}^0\end{Bmatrix}-\begin{pmatrix}B_{11}&B_{12}&B_{16}\\B_{12}&B_{22}&B_{26}\\B_{16}&B_{26}&B_{66}\end{pmatrix}\begin{Bmatrix}\chi_r\\\chi_\varphi\\2\chi_{r\varphi}\end{Bmatrix} \tag{19}$$

$$\begin{Bmatrix}M_r\\M_\varphi\\M_{r\varphi}\end{Bmatrix}=\begin{pmatrix}B_{11}&B_{12}&B_{16}\\B_{12}&B_{22}&B_{26}\\B_{16}&B_{26}&B_{66}\end{pmatrix}\begin{Bmatrix}\varepsilon_r^0\\\varepsilon_\varphi^0\\\gamma_{r\varphi}^0\end{Bmatrix}-\begin{pmatrix}D_{11}&D_{12}&D_{16}\\D_{12}&D_{22}&D_{26}\\D_{16}&D_{26}&D_{66}\end{pmatrix}\begin{Bmatrix}\chi_r\\\chi_\varphi\\2\chi_{r\varphi}\end{Bmatrix} \tag{20}$$

in which

$$A_s=\int_{-h/2}^{h/2}\tilde{Q}_s dz,\quad B_s=\int_{-h/2}^{h/2}\tilde{Q}_s z dz,\quad D_s=\int_{-h/2}^{h/2}\tilde{Q}_s z^2 dz,\quad s=\{11,12,22,16,26,66\} \tag{21}$$

Finally, one may express the governing equations for an annular sector plate rested on elastic foundation with parameters (k_w, k_p) as

$$\frac{\partial N_r}{\partial r}+\frac{1}{r}\frac{\partial N_{r\theta}}{\partial\theta}+\frac{1}{r}(N_r-N_\theta)=I_0\frac{\partial^2 u}{\partial t^2} \tag{22}$$

$$\frac{\partial N_{r\theta}}{\partial r}+\frac{1}{r}\frac{\partial N_\theta}{\partial\theta}+\frac{2}{r}N_{r\theta}=I_0\frac{\partial^2 v}{\partial t^2} \tag{23}$$

$$\begin{aligned}&\frac{\partial^2 M_r}{\partial r^2}+\frac{2}{r}\frac{\partial M_r}{\partial r}+\frac{2}{r}\frac{\partial^2 M_{r\theta}}{\partial r\partial\theta}+\frac{2}{r^2}\frac{\partial M_{r\theta}}{\partial\theta}\\&+\frac{1}{r^2}\frac{\partial^2 M_\theta}{\partial\theta^2}-\frac{1}{r}\frac{\partial M_\theta}{\partial r}+N_r\frac{\partial^2 w}{\partial r^2}\\&-2N_{r\theta}(\frac{1}{r^2}\frac{\partial w}{\partial\theta}-\frac{1}{r}\frac{\partial^2 w}{\partial r\partial\theta})+N_\theta(\frac{1}{r}\frac{\partial w}{\partial r}+\frac{1}{r^2}\frac{\partial^2 w}{\partial\theta^2})\\&-k_w w+k_P(\frac{\partial^2 w}{\partial r^2}+\frac{1}{r}\frac{\partial w}{\partial r}+\frac{1}{r^2}\frac{\partial^2 w}{\partial\theta^2})\\&=I_0\frac{\partial^2 w}{\partial t^2}+f(t)\end{aligned} \tag{24}$$

where $f(t)=F\cos(\omega t)$ and $I_0=\int_{-h/2}^{h/2}\rho dz$. Note that F is force amplitude and ω is excitation frequency. By substituting Eqs. (19)-(20) into Eqs. (22) and (24), nonlinear governing equations in terms of strain components can be expressed as follows

$$\begin{aligned}&\frac{\partial}{\partial r}[A_{11}\varepsilon_r^0+A_{12}\varepsilon_\varphi^0+A_{16}\gamma_{r\varphi}^0\\&-B_{11}\chi_r-B_{21}\chi_\varphi-2B_{16}\chi_{r\varphi}]\\&+\frac{1}{r}\frac{\partial}{\partial\theta}[A_{16}\varepsilon_r^0+A_{26}\varepsilon_\varphi^0+A_{66}\gamma_{r\varphi}^0\\&-B_{16}\chi_r-B_{26}\chi_\varphi-2B_{66}\chi_{r\varphi}]\\&+\frac{1}{r}(A_{11}\varepsilon_r^0+A_{12}\varepsilon_\varphi^0+A_{16}\gamma_{r\varphi}^0\\&-B_{11}\chi_r-B_{21}\chi_\varphi-2B_{16}\chi_{r\varphi}\\&-A_{12}\varepsilon_r^0-A_{22}\varepsilon_\varphi^0-A_{26}\gamma_{r\varphi}^0\\&+B_{12}\chi_r+B_{22}\chi_\varphi+2B_{26}\chi_{r\varphi})=I_0\frac{\partial^2 u}{\partial t^2}\end{aligned} \tag{25}$$

$$\begin{aligned}&\frac{\partial}{\partial r}[A_{16}\varepsilon_r^0+A_{26}\varepsilon_\varphi^0+A_{66}\gamma_{r\varphi}^0\\&-B_{16}\chi_r-B_{26}\chi_\varphi-2B_{66}\chi_{r\varphi}]\\&+\frac{1}{r}\frac{\partial}{\partial\theta}[A_{12}\varepsilon_r^0+A_{22}\varepsilon_\varphi^0+A_{26}\gamma_{r\varphi}^0\\&-B_{12}\chi_r-B_{22}\chi_\varphi-2B_{26}\chi_{r\varphi}]\\&+\frac{2}{r}[A_{16}\varepsilon_r^0+A_{26}\varepsilon_\varphi^0+A_{66}\gamma_{r\varphi}^0\\&-B_{16}\chi_r-B_{26}\chi_\varphi-2B_{66}\chi_{r\varphi}]=I_0\frac{\partial^2 v}{\partial t^2}\end{aligned} \tag{26}$$

$$\begin{aligned}&\frac{\partial^2}{\partial r^2}[B_{11}\varepsilon_r^0+B_{12}\varepsilon_\varphi^0+B_{16}\gamma_{r\varphi}^0\\&-D_{11}\chi_r+D_{12}\chi_\varphi-2D_{16}\chi_{r\varphi}]\\&+\frac{2}{r}\frac{\partial}{\partial r}[B_{11}\varepsilon_r^0+B_{12}\varepsilon_\varphi^0+B_{16}\gamma_{r\varphi}^0\\&-D_{11}\chi_r+D_{12}\chi_\varphi-2D_{16}\chi_{r\varphi}]\\&+\frac{2}{r}\frac{\partial^2}{\partial r\partial\theta}[B_{16}\varepsilon_r^0+B_{26}\varepsilon_\varphi^0+B_{66}\gamma_{r\varphi}^0\\&-D_{16}\chi_r-D_{26}\chi_\varphi-2D_{66}\chi_{r\varphi}]\\&+\frac{2}{r^2}\frac{\partial}{\partial\theta}[B_{16}\varepsilon_r^0+B_{26}\varepsilon_\varphi^0+B_{66}\gamma_{r\varphi}^0\\&-D_{16}\chi_r-D_{26}\chi_\varphi-2D_{66}\chi_{r\varphi}]\\&+\frac{1}{r^2}\frac{\partial^2}{\partial\theta^2}[B_{12}\varepsilon_r^0+B_{22}\varepsilon_\varphi^0+B_{26}\gamma_{r\varphi}^0\\&-D_{12}\chi_r-D_{22}\chi_\varphi-2D_{26}\chi_{r\varphi}]\\&-\frac{1}{r}\frac{\partial}{\partial r}[B_{12}\varepsilon_r^0+B_{22}\varepsilon_\varphi^0+B_{26}\gamma_{r\varphi}^0\\&-D_{12}\chi_r-D_{22}\chi_\varphi-2D_{26}\chi_{r\varphi}]\\&+[A_{11}\varepsilon_r^0+A_{12}\varepsilon_\varphi^0+A_{16}\gamma_{r\varphi}^0-B_{11}\chi_r\\&-B_{21}\chi_\varphi-2B_{16}\chi_{r\varphi}]\frac{\partial^2 w}{\partial r^2}\\&-2[A_{16}\varepsilon_r^0+A_{26}\varepsilon_\varphi^0+A_{66}\gamma_{r\varphi}^0-B_{16}\chi_r\\&-B_{26}\chi_\varphi-2B_{66}\chi_{r\varphi}](\frac{1}{r^2}\frac{\partial w}{\partial\theta}-\frac{1}{r}\frac{\partial^2 w}{\partial r\partial\theta})\\&+[A_{12}\varepsilon_r^0+A_{22}\varepsilon_\varphi^0+A_{26}\gamma_{r\varphi}^0-B_{12}\chi_r\\&-B_{22}\chi_\varphi-2B_{26}\chi_{r\varphi}](\frac{1}{r}\frac{\partial w}{\partial r}+\frac{1}{r^2}\frac{\partial^2 w}{\partial\theta^2})\\&-k_w w+k_P(\frac{\partial^2 w}{\partial r^2}+\frac{1}{r}\frac{\partial w}{\partial r}+\frac{1}{r^2}\frac{\partial^2 w}{\partial\theta^2})\\&=I_0\frac{\partial^2 w}{\partial t^2}+f(t)\end{aligned} \tag{27}$$

4. Solution procedure

Herein, the solution of nonlinear governing equations of multi-scale annular sector plate has been presented. Firstly, it should be noted that the edges of annular sector plate are simply-supported based upon following conditions

$$\begin{aligned} &w = M_r = N_{r\theta} = 0 \ \text{ at r=r}_0 \\ &w = M_\theta = N_{r\theta} = 0 \ \text{ at } \theta=0,\psi \end{aligned} \tag{28}$$

According to the thin sector plate formulation, the displacement field may be selected as

$$u = \sum_{i=1}^{\infty}\sum_{j=1}^{\infty} U_{ij}(t)\frac{\partial H_i(r)}{\partial r}R_j(\varphi) \tag{29}$$

$$v = \sum_{i=1}^{\infty}\sum_{j=1}^{\infty} V_{ij}(t)H_i(r)\frac{\partial R_j(\varphi)}{\partial \varphi} \tag{30}$$

$$w = \sum_{i=1}^{\infty}\sum_{j=1}^{\infty} W_{ij}(t)H_i(r)R_j(\varphi) \tag{31}$$

where (U ,V ,W) are the displacements amplitudes and the functions H_i and R_j are the test functions which are selected as

$$\begin{aligned} &H_i(r) = \sin\frac{i\pi(r-r_0)}{r_1-r_0}, \\ &R_j(\varphi) = \sin\left(\frac{j\pi\varphi}{\psi}\right) \end{aligned} \tag{32}$$

Arranging the governing equations as Y_i (u, v, w)=0 with (i=1,2,3) and inserting field components presented as Eqs. (29)-(31) into Y_i yields following equations with the use of Galerkin's technique

$$\int_{r_0}^{r_1}\int_0^{\psi} Y_1\frac{\partial H_i(r)}{\partial r}R_j(\varphi)rdrd\varphi = 0 \tag{33}$$

$$\int_{r_0}^{r_1}\int_0^{\psi} Y_2 H_i(r)\frac{\partial R_j(\varphi)}{\partial \varphi}rdrd\varphi = 0 \tag{34}$$

$$\int_{r_0}^{r_1}\int_0^{\psi} Y_3 H_i(r)R_j(\varphi)rdrd\varphi = 0 \tag{35}$$

After solving Eqs. (33)-(35) by neglecting in-plane inertias, three governing equations will be derived

$$K_{11}U + K_{21}V + K_{31}W + G_1W^2 = 0 \tag{36}$$

$$K_{12}U + K_{22}V + K_{32}W + G_2W^2 = 0 \tag{37}$$

$$\begin{aligned} &K_{13}U + K_{23}V + K_{33}W + G_3W^2 \\ &+G_4W^3 + n_1UW + n_2VW + M\ddot{W} = F\cos(\omega t) \end{aligned} \tag{38}$$

in which K_{ij} are stiffness matrix components; M is mass matrix and G_i are nonlinear stiffness matrices. With the use of Eqs. (36) and (37), U and V are calculated as

$$\begin{aligned} U &= \frac{K_{21}K_{32}-K_{22}K_{31}}{K_{11}K_{22}-K_{12}K_{21}}W \\ &+\frac{G_2K_{21}-G_1K_{22}}{K_{11}K_{22}-K_{12}K_{21}}W^2 \\ V &= \frac{K_{12}K_{31}-K_{11}K_{32}}{K_{11}K_{22}-K_{12}K_{21}}W \\ &+\frac{G_1K_{12}-G_2K_{11}}{K_{11}K_{22}-K_{12}K_{21}}W^2 \end{aligned} \tag{39}$$

Therefore, Eq. (38), with the aid of Eq. (39) can be reduced to below equation

$$\ddot{W} + \frac{T_1}{M}W + \frac{T_2}{M}W|W| + \frac{T_3}{M}W^3 = \frac{F}{M}\cos(\omega t) \tag{40}$$

for which

$$\begin{aligned} T_1 &= K_{13}\frac{K_{21}K_{32}-K_{22}K_{31}}{K_{11}K_{22}-K_{12}K_{21}} \\ &+K_{33}+K_{23}\frac{K_{12}K_{31}-K_{11}K_{32}}{K_{11}K_{22}-K_{12}K_{21}} \\ T_2 &= +G_3+K_{13}\frac{G_2K_{21}-G_1K_{22}}{K_{11}K_{22}-K_{12}K_{21}} \\ &+K_{23}\frac{G_1K_{12}-G_2K_{11}}{K_{11}K_{22}-K_{12}K_{21}}+n_1\frac{K_{21}K_{32}-K_{22}K_{31}}{K_{11}K_{22}-K_{12}K_{21}} \\ &+n_2\frac{K_{12}K_{31}-K_{11}K_{32}}{K_{11}K_{22}-K_{12}K_{21}} \\ T_3 &= +G_4+n_1\frac{G_2K_{21}-G_1K_{22}}{K_{11}K_{22}-K_{12}K_{21}} \\ &+n_2\frac{G_1K_{12}-G_2K_{11}}{K_{11}K_{22}-K_{12}K_{21}} \end{aligned} \tag{41}$$

Exact solution of above equation can be introduced based on Jacobi elliptic function (cn) as (Feng and Meng 2017)

$$W = \tilde{W}cn(\vartheta t, k^2) \tag{42}$$

Note that k^2 is the modulus of the elliptic function; $\tilde{W}$ is vibration amplitude. It should be pointed out that ϑ is the frequency of elliptic function. Based on the Fourier expansion, the Jacobi elliptic function (cn) can be expressed as a series of corresponding trigonometric function as

$$cn(\vartheta t, k^2) = \frac{2\pi}{kK}\sum_{r=0}^{\infty}\frac{q^{r+\frac{1}{2}}}{1+q^{2r+1}}\cos\left((2r+1)\frac{\pi\vartheta t}{2K}\right) \tag{43}$$

Then, inserting Eq. (42) into Eq. (40) and with the use of series expansion for $cn|cn| \approx a_0cn + a_1cn^3$ one can express that

Table 2 Validation of vibration frequency of nano-composite annular plates for various ratios of inner to outer radius (h/r_1=0.05)

	Liu *et al.* (2019)	Present
r_0/r_1=0.1	0.0228	0.0228
r_0/r_1=0.2	0.0264	0.0265
r_0/r_1=0.3	0.0332	0.0334

$$-\tilde{W}\vartheta^2 cn(1-2k^2+2k^2cn^2)+\frac{T_1}{M}\tilde{W}cn+\frac{T_3}{M}\tilde{W}^3cn^3 +\frac{T_2}{M}\tilde{W}\left|\tilde{W}\right|(a_0cn+a_1cn^3)=\frac{F}{M}\cos(\omega t) \tag{44}$$

Equating the terms having same orders of the elliptic function *cn*, yields two coupled algebraic equations. Form obtained equation one can get to

$$k^2=\frac{\frac{T_2}{M}\left|\tilde{W}\right|a_1+\frac{T_3}{M}\tilde{W}^2}{2\left(\frac{T_1}{M}+\frac{T_2}{M}\left|\tilde{W}\right|(a_0+a_1)+\frac{T_3}{M}\tilde{W}^2\right)} \tag{45}$$

The vibration frequency depends on the period of elliptic function, $\Upsilon=2\pi/T$ in which

$$T=\frac{4K(k)}{\vartheta} \tag{46}$$

where

$$K=\int_0^{\pi/2}\frac{d\theta}{\sqrt{1-k^2\sin^2\theta}} \tag{47}$$

Also, some normalized parameters can be introduced in this paper such as

$$\Omega=\Upsilon 10^3h^2\sqrt{\frac{\rho_m}{E_mh^2}}\,,\tilde{F}=F\frac{h^2}{A_{11}},\quad K_w=\frac{k_wh^4}{D_{11}},K_p=\frac{k_ph^2}{D_{11}} \tag{48}$$

5. Results and discussions

Presented in this section is nonlinear forced vibration characteristics of a multi-scale epoxy/CNT/fiberglass annular sector plate subjected to transverse harmonic load. In previous sections, a Mori-Tanaka model was employed for evaluating multi-scale material properties. Also, Jacobi elliptic functions were used for solving the governing equations and deriving forced vibration curves of the multi-scale annular sector. This section provide new findings for demonstrating the significance of CNT distribution, geometric nonlinearity, applied force, fiberglass volume, open angle and fiber directions on forced vibration characteristics of multi-scale annular sector plates.

Based on various values of inner to outer radius ratio (r_0/r_1) of nano-composite annular plate, Table 2 presents the validation of vibration frequency with that of Liu et al. (2019). In this table it is assumed that r_0/r_1=0.1, 0.2 and 0.3 and plate thickness is h/r_1=0.05. Also, uniform dispersion of carbon-based inclusion within the matrix is assumed. One can see the excellent agreement among obtained frequencies and the results provided by Liu *et al*. (2019).

Forced vibration curves of multi-scale annular sector for various CNT weight fraction (W_{cnt}) are shown in Fig. 4 when the open angle is considered as $\psi=\pi$. Also, the normalized value of applied for is considered as $\tilde{F}$=0.0001. This figure shows the normalized deflection ($\tilde{W}/h$) variation of annular sector with excitation frequency. It is obvious that deflection value is increasing with respect to excitation frequency and resonance occurs at a particular value of excitation frequency. It is also seen that frequency-amplitude curves of annular sector moves to the right by increase of CNT weight fraction. This means that resonance occurs at higher values of excitation frequency when the CNT weight fraction increases. So, adding CNT into the matrix will improve forced vibration characteristics of the annular sector plate.

Based on various values of fiberglass volume (V_f), Fig. 5 illustrates the variation of frequency-deflection curves of annular sector plate with open angle $\psi=\pi$. The weight fraction of CNTs is chosen to be W_{cnt}=0.2%. Outer radius of the sector is considered as r_1=100h while inner radius is $r_0=0.2r_1$. This figure indicates that higher values for fiberglass volume result in greater excitation frequencies due to increased stiffness of the annular sector. Therefore, it can be concluded that both fiberglass and CNT content can affect forced vibration behavior of annular sector.

Forced vibration curves of multi-scale annular sector for various open angles are plotted in Fig. 6 by assuming that W_{cnt}=0.2% and V_f=0.1. Annular sectors with different values of open angle have diverse nonlinear vibration behaviors. Actually, annular sector with lower open angle has more deviation to the right due to increase of nonlinear effects. Thus, as the open angle increases the nonlinear effects become less prominent and frequency-amplitude curves have less deviations. In this figure, the most notable influence of nonlinearity is obtained when ψ=30 degree.

Based on various values of fiber orientation (θ), Fig. 5 depicts the variation of normalized deflection of annular sector with respect to excitation frequency. It is assumed that W_{cnt}=0.2% and V_f=0.1. It must be pointed out that θ=0 results in fiber direction parallel to radial axis. One can see that increasing in orientation angle yields lower excitation frequency. Accordingly, as the value of fiber orientation is greater, the structural stiffness of annular sector is decreased. Hence, the forced vibration behaviors of annular sectors made of multi-scale composites rely on the orientations of included fibers.

Fig. 8 highlights that the ratio of length to diameter ($\alpha=l/D$) of CNTs has a major role in forced vibration behavior of multi-scale annular sectors. The weight fraction of CNTs is chosen to be W_{cnt}=0.2%. Outer radius of the sector is considered as r_1=100h while inner radius is $r_0=0.2r_1$.

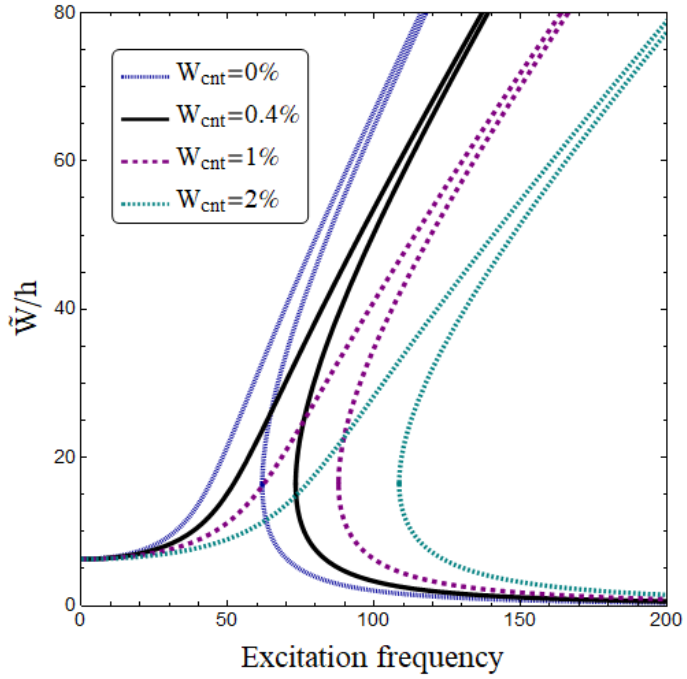

Fig. 4 Forced vibration curves of multi-scale annular sector for various CNT weight fraction (r_1=100h, r_0=0.2r_1, V_f=0, K_w=0.01, ψ=π, $\tilde{F}$=0.0001, α=50)

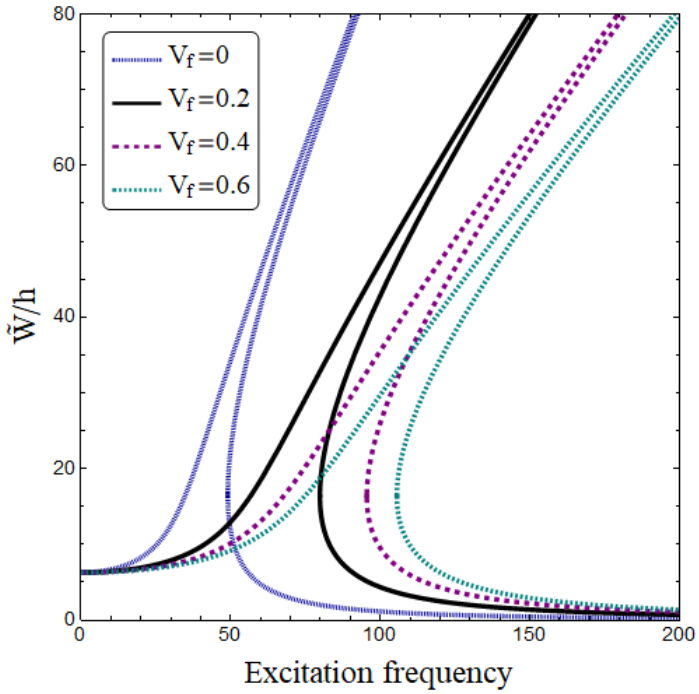

Fig. 5 Forced vibration curves of multi-scale annular sector for various fiberglass volume (r_1=100h, r_0=0.2r_1, W_{cnt}=0.2%, K_w=0.01, K_p=0.001, ψ=π, α=50)

It can be seen that by increasing the magnitude of CNT length-to-diameter ratio, the excitation frequency increases. It means that larger CNTs are added to the matrix. Therefore, as *l/D* becomes greater, each CNT is longer and the composites become more influenced by CNT geometry.

In Fig. 9, the variation of normalized deflection of annular sector with respect to excitation frequency is plotted according to diverse values for normalized force amplitude $\tilde{F}$. Foundation parameters are set as K_w=0.01, K_p=0.001. It is clear that force amplitude has no impact on the magnitude

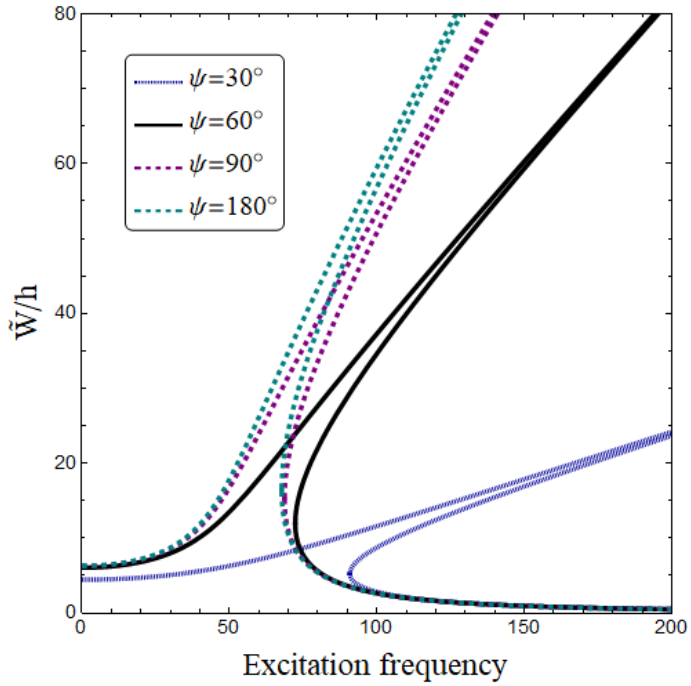

Fig. 6 Forced vibration curves of multi-scale annular sector for various open angles (r_1=100h, r_0=0.2r_1, W_{cnt}=0.2%, K_w=0.01)

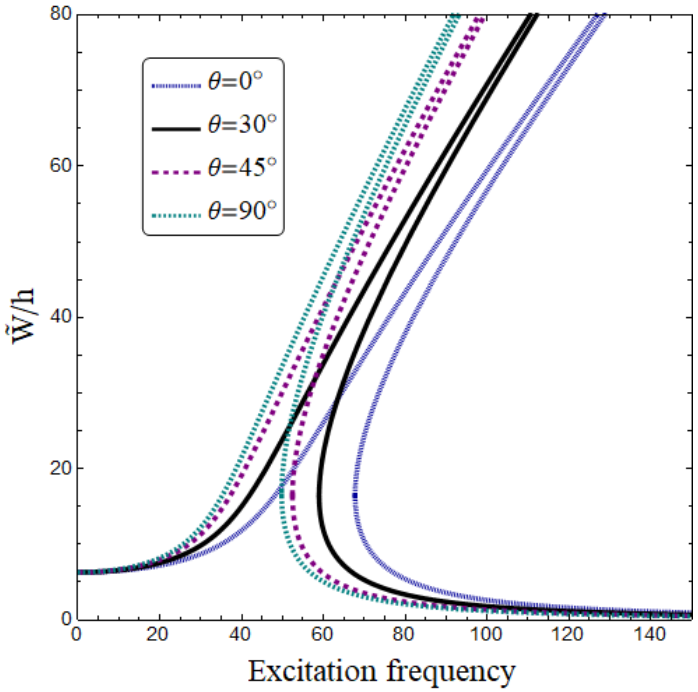

Fig. 7 Forced vibration curves of multi-scale annular sector for various fiber angles (r_1=100h, r_0=0.2r_1, W_{cnt}=0.2%, V_f=0.1, K_w=0.01, K_p=0.001, ψ=π)

of excitation frequency, but it greatly affects the values of deflections. Indeed, higher values for normalized force amplitude yield larger deflections, but un-varied resonance frequency location. So, in nonlinear analysis of forced vibrations of annular sector plates, the magnitude of force amplitude has a key load in determining the response branches.

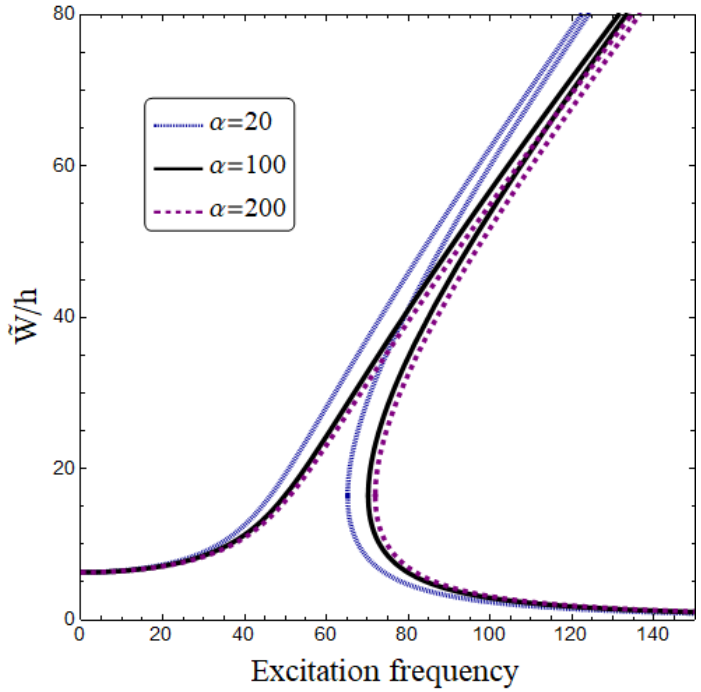

Fig. 8 Forced vibration curves of multi-scale annular sector for various CNT length-to-diameter ratio (r_1=100h, r_0=0.2r_1, W_{cnt}=0.2%, V_f=0.1, K_w=0.01, K_p=0.001, ψ=π)

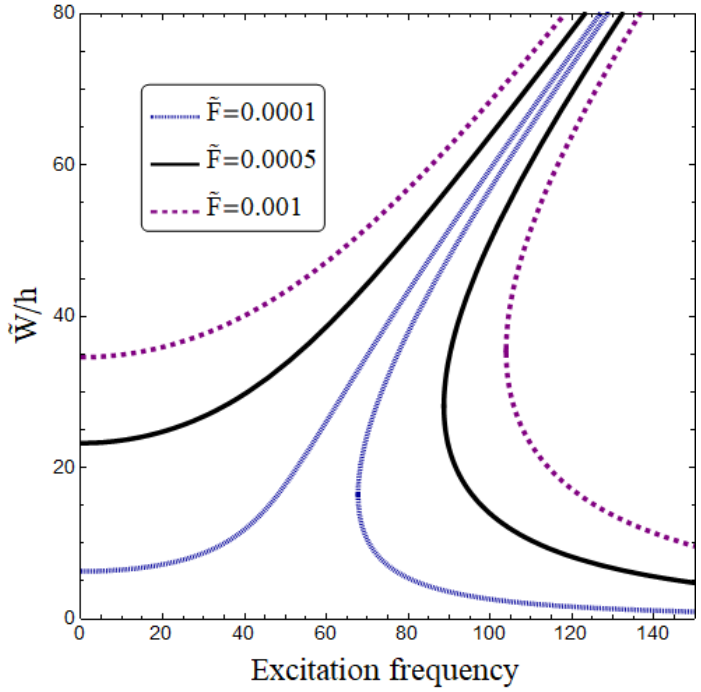

Fig. 9 Forced vibration curves of multi-scale annular sector for various force amplitude (r_1=100h, r_0=0.2r_1, W_{cnt}=0.2%, V_f=0.1, K_w=0.01, K_p=0.001, ψ=π)

Fig. 10 depicts forced vibration properties of multi-scale annular sector plate affected by diverse values of outer radius (r_1) at fixed values of r_0=0.2r_1, W_{cnt}=0.2%, V_f=0.1, K_w=0.01, K_p=0.001 and ψ=π. Outer radius of the sector has a great influences on deviation of frequency-amplitude curves. Actually, more deviation is observed for lower values of outer radius which means that nonlinear effects are more announced. So, the geometry of annular sector is

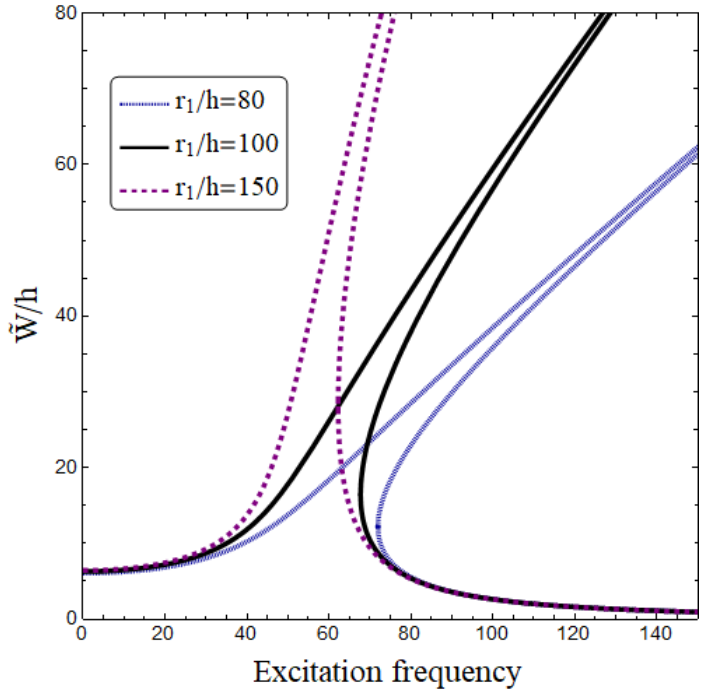

Fig. 10 Forced vibration curves of multi-scale annular sector for various sector radius (r_0=0.2r_1, W_{cnt}=0.2%, V_f=0.1, K_w=0.01, K_p=0.001, ψ=π)

very important for determining the forced vibration properties.

6. Conclusions

Based on an analytical trend, the presented article examined nonlinear forced vibrations of annular sector plates made of multi-scale materials. The multi-scale composite is consist of epoxy, random CNTs and glass fibers which were included into the calculations based on Mori-Tanaka scheme. Jacobi elliptic functions were employed for determining the frequency-amplitude curves of annular sector. In the below statements, new findings are introduced:

- The resonance occurs at higher values of excitation frequency when the CNT weight fraction increases.
- Higher values for fiberglass volume result in greater excitation frequencies due to increased stiffness of the annular sector.
- As the open angle increases the nonlinear effects become less prominent and frequency-amplitude curves have less deviations.
- Increasing in fiber orientation angle yields lower excitation frequency.
- By increasing the magnitude of CNT length-to-diameter ratio, the excitation frequency increases.
- Nonlinear effects become more prominent as the value of sector outer radius reduces.

Acknowledgements

The first and second authors would like to thank FPQ (Fidar project Qaem) for providing the fruitful and useful help.

References

Abualnour, M., Chikh, A., Hebali, H., Kaci, A., Tounsi, A., Bousahla, A.A. and Tounsi, A. (2019), "Thermomechanical analysis of antisymmetric laminated reinforced composite plates using a new four variable trigonometric refined plate theory. *Comput. Concrete*, **24**(6), 489-498. https://doi.org/10.12989/cac.2019.24.6.489.

Addou, F.Y., Meradjah, M., Bousahla, A.A., Benachour, A., Bourada, F., Tounsi, A. and Mahmoud, S.R. (2019), "Influences of porosity on dynamic response of FG plates resting on Winkler/Pasternak/Kerr foundation using quasi 3D HSDT. *Comput. Concrete*, **24**(4), 347-367. https://doi.org/10.12989/cac.2019.24.4.347.

Ahmed, R.A., Fenjan, R.M. and Faleh, N.M. (2019), "Analyzing post-buckling behavior of continuously graded FG nanobeams with geometrical imperfections", *Geomech. Eng.*, **17**(2), 175-180. https://doi.org/10.12989/gae.2019.17.2.175.

Azimi, M., Mirjavadi, S.S., Shafiei, N. and Hamouda, A.M.S. (2017), "Thermo-mechanical vibration of rotating axially functionally graded nonlocal Timoshenko beam", *Appl. Phys. A*, **123**(1), 104.

Azimi, M., Mirjavadi, S.S., Shafiei, N., Hamouda, A.M.S. and Davari, E. (2018), "Vibration of rotating functionally graded Timoshenko nano-beams with nonlinear thermal distribution", *Mech. Adv. Mater. Struct.*, **25**(6), 467-480.

Barati, M.R. and Zenkour, A.M. (2017), "Post-buckling analysis of refined shear deformable graphene platelet reinforced beams

with porosities and geometrical imperfection", *Compos. Struct.*, **181**, 194-202. https://doi.org/10.1016/j.compstruct.2017.08.082.

Balubaid, M., Tounsi, A., Dakhel, B. and Mahmoud, S.R. (2019), "Free vibration investigation of FG nanoscale plate using nonlocal two variables integral refined plate theory", *Comput. Concrete*, **24**(6), 579-586. https://doi.org/10.12989/cac.2019.24.6.579.

Berghouti, H., Adda Bedia, E.A., Benkhedda, A. and Tounsi, A. (2019), "Vibration analysis of nonlocal porous nanobeams made of functionally graded material", *Adv. Nano Res.*, **7**(5), 351-364. https://doi.org/10.12989/anr.2019.7.5.351.

Bouamoud, A., Boucham, B., Bourada, F., Houari, M.S.A. and Tounsi, A. (2019), "Thermomechanical bending investigation of FGM sandwich plates using four shear deformation plate theory", *Steel Compos. Struct.*, **32**(5), 611-632. https://doi.org/10.12989/scs.2019.32.5.611.

Boulefrakh, L., Hebali, H., Chikh, A., Bousahla, A.A., Tounsi, A. and Mahmoud, S.R. (2019), "The effect of parameters of visco-Pasternak foundation on the bending and vibration properties of a thick FG plate", *Geomech. Eng.*, **18**(2), 161-178. https://doi.org/10.12989/gae.2019.18.2.161.

Draiche, K., Bousahla, A.A., Tounsi, A., Alwabli, A.S., Tounsi, A. and Mahmoud, S.R. (2019), "Static analysis of laminated reinforced composite plates using a simple first-order shear deformation theory", *Comput. Concrete*, **24**(4), 369-378. https://doi.org/10.12989/cac.2019.24.4.369.

Draoui, A., Zidour, M., Tounsi, A. and Adim, B. (2019), "Static and dynamic behavior of nanotubes-reinforced sandwich plates using (FSDT)", *J. Nano Res.*, **57**, 117-135. https://doi.org/10.4028/www.scientific.net/JNanoR.57.117.

Dai, T., Yang, Y., Dai, H.L., Tang, H. and Lin, Z.Y. (2019), "Hygrothermal mechanical behaviors of a porous FG-CRC annular plate with variable thickness considering aggregation of CNTs", *Compos. Struct.*, 215, 198-213. https://doi.org/10.1016/j.compstruct.2019.02.061.

Dong, Y.H., Li, Y.H., Chen, D. and Yang, J. (2018), "Vibration characteristics of functionally graded graphene reinforced porous nanocomposite cylindrical shells with spinning motion", *Compos. Part B: Eng.*, **145**, 1-13.

Ebrahimi, F., Jafari, A. and Mahesh, V. (2019), "Assessment of porosity influence on dynamic characteristics of smart heterogeneous magneto-electro-elastic plates", *Struct. Eng. Mech.*, **72**(1), 113-129. https://doi.org/10.12989/sem.2019.72.1.113.

Feng, C., Kitipornchai, S. and Yang, J. (2017), "Nonlinear bending of polymer nanocomposite beams reinforced with non-uniformly distributed graphene platelets (GPLs)", *Compos. Part B: Eng.*, **110**, 132-140.

Feng, Q. and Meng, F. (2017), "Traveling wave solutions for fractional partial differential equations arising in mathematical physics by an improved fractional Jacobi elliptic equation method", *Math. Method. Appl. Sci.*, **40**(10), 3676-3686. https://doi.org/10.1002/mma.4254.

Hellal, H., Bourada, M., Hebali, H., Bourada, F., Tounsi, A., Bousahla, A.A. and Mahmoud, S.R. (2019), "Dynamic and stability analysis of functionally graded material sandwich plates in hygro-thermal environment using a simple higher shear deformation theory", *J. Sandw. Struct. Mater.*, 1099636219845841. https://doi.org/10.1177%2F1099636219845841.

Hussain, M., Naeem, M.N., Tounsi, A. and Taj, M. (2019), "Nonlocal effect on the vibration of armchair and zigzag SWCNTs with bending rigidity", *Adv. Nano Res.*, **7**(6), 431. https://doi.org/10.12989/anr.2019.7.6.431.

Houari, T., Bessaim, A., Houari, M.S.A., Benguediab, M. and Tounsi, A. (2018), "Bending analysis of advanced composite plates using a new quasi 3D plate theory", *Steel Compos. Struct.*, **26**(5), 557-572. https://doi.org/10.12989/scs.2018.26.5.557.

Kaddari, M., Kaci, A., Bousahla, A.A., Tounsi, A., Bourada, F., Bedia, E.A. and Al-Osta, M.A. (2020), "A study on the structural behaviour of functionally graded porous plates on elastic foundation using a new quasi-3D model: bending and free vibration analysis", *Comput. Concrete*, **25**(1), 37. https://doi.org/10.12989/cac.2020.25.1.037.

Khiloun, M., Bousahla, A.A., Kaci, A., Bessaim, A., Tounsi, A. and Mahmoud, S.R. (2019), "Analytical modeling of bending and vibration of thick advanced composite plates using a four-variable quasi 3D HSDT", *Eng. with Comput.*, 1-15. https://doi.org/10.1007/s00366-019-00732-1.

Khosravi, F., Hosseini, S.A. and Tounsi, A. (2020), "Torsional dynamic response of viscoelastic SWCNT subjected to linear and harmonic torques with general boundary conditions via Eringen's nonlocal differential model", *Eur. Physical J. Plus*, **135**(2), 183. https://doi.org/10.1140/epjp/s13360-020-00207-z.

Kazakov, I.A., Krasnovskii, A.N. and Kishuk, P.S. (2019), "The influence of randomly oriented CNTs on the elastic properties of unidirectionally aligned composites", *Mech. Mater.*, **134**, 54-60. https://doi.org/10.1016/j.mechmat.2019.04.002.

Keleshteri, M.M., Asadi, H. and Aghdam, M.M. (2019), "Nonlinear bending analysis of FG-CNTRC annular plates with variable thickness on elastic foundation", *Thin-Wall. Struct.*, **135**, 453-462. https://doi.org/10.1016/j.tws.2018.11.020.

Liu, D., Li, Z., Kitipornchai, S. and Yang, J. (2019), "Three-dimensional free vibration and bending analyses of functionally graded graphene nanoplatelets-reinforced nanocomposite annular plates", *Compos. Struct.*, **229**, 111453. https://doi.org/10.1016/j.compstruct.2019.111453.

Mahesh, V., Sagar, P.J. and Kattimani, S. (2018), "Influence of coupled fields on free vibration and static behavior of functionally graded magneto-electro-thermo-elastic plate", *J. Intel. Mat. Syst. Str.*, **29**(7), 1430-1455.

Mahesh, V. and Kattimani, S. (2019), "Finite element simulation of controlled frequency response of skew multiphase magneto-electro-elastic plates", *J. Intel. Mat. Syst. Str.*, **30**(12), 1757-1771.

Mahesh, V., Kattimani, S., Harursampath, D. and Trung, N.T. (2019), "Coupled evaluation of the free vibration characteristics of magneto-electro-elastic skew plates in hygrothermal environment", *Smart Struct. Syst.*, **24**(2), 267-292. https://doi.org/10.12989/sss.2019.24.2.267.

Mahmoudi, A., Benyoucef, S., Tounsi, A., Benachour, A., Adda Bedia, E.A. and Mahmoud, S.R. (2019), "A refined quasi-3D shear deformation theory for thermo-mechanical behavior of functionally graded sandwich plates on elastic foundations", *J. Sandw. Struct. Mater.*, **21**(6), 1906-1929. https://doi.org/10.1177%2F1099636217727577.

Medani, M., Benahmed, A., Zidour, M., Heireche, H., Tounsi, A., Bousahla, A.A. and Mahmoud, S.R. (2019), "Static and dynamic behavior of (FG-CNT) reinforced porous sandwich plate using energy principle", *Steel Compos. Struct.*, **32**(5), 595-610. https://doi.org/10.12989/scs.2019.32.5.595.

Meksi, R., Benyoucef, S., Mahmoudi, A., Tounsi, A., Adda Bedia, E.A. and Mahmoud, S.R. (2019), "An analytical solution for bending, buckling and vibration responses of FGM sandwich plates", *J. Sandw. Struct. Mater,*, **21**(2), 727-757. https://doi.org/10.1177%2F1099636217698443.

Marynowski, K. (2017), "Free vibration analysis of an axially moving multiscale composite plate including thermal effect", *Int. J. Mech. Sci.*, **120**, 62-69. https://doi.org/10.1016/j.ijmecsci.2016.11.013.

Mirjavadi, S.S., Rabby, S., Shafiei, N., Afshari, B.M. and Kazemi, M. (2017), "On size-dependent free vibration and thermal

buckling of axially functionally graded nanobeams in thermal environment", *Appl. Phys. A*, **123**(5), 315.

Mirjavadi, S.S., Afshari, B.M., Shafiei, N., Hamouda, A.M.S. and Kazemi, M. (2017), "Thermal vibration of two-dimensional functionally graded (2D-FG) porous Timoshenko nanobeams", *Steel Compos. Struct.*, **25**(4), 415-426. https://doi.org/10.12989/scs.2017.25.4.415.

Mirjavadi, S.S., Afshari, B.M., Barati, M.R. and Hamouda, A.M. S. (2018), "Strain gradient based dynamic response analysis of heterogeneous cylindrical microshells with porosities under a moving load", *Mater. Res. Express*, **6**(3), 035029.

Mirjavadi, S.S., Afshari, B.M., Khezel, M., Shafiei, N., Rabby, S. and Kordnejad, M. (2018), "Nonlinear vibration and buckling of functionally graded porous nanoscaled beams", *J. Brazilian Soc. Mech. Sci. Eng.*, **40**(7), 352.

Mirjavadi, S.S., Forsat, M., Hamouda, A.M.S. and Barati, M.R. (2019), "Dynamic response of functionally graded graphene nanoplatelet reinforced shells with porosity distributions under transverse dynamic loads", *Mater. Res. Express*, **6**(7), 075045.

Mirjavadi, S.S., Forsat, M., Nikookar, M., Barati, M.R. and Hamouda, A.M.S. (2019), "Nonlinear forced vibrations of sandwich smart nanobeams with two-phase piezo-magnetic face sheets", *Eur. Phys. J. Plus*, **134**(10), 508.

Mirjavadi, S.S., Afshari, B.M., Barati, M.R. and Hamouda, A.M.S. (2019), "Transient response of porous FG nanoplates subjected to various pulse loads based on nonlocal stress-strain gradient theory", *Eur. J. Mech.-A/Solids*, **74**, 210-220.

Mirjavadi, S.S., Afshari, B.M., Barati, M.R. and Hamouda, A.M.S. (2019), "Nonlinear free and forced vibrations of graphene nanoplatelet reinforced microbeams with geometrical imperfection", *Microsyst. Technologies*, **25**, 3137-3150.

Mirjavadi, S.S., Forsat, M., Barati, M.R., Abdella, G.M., Hamouda, A.M.S., Afshari, B.M. and Rabby, S. (2019), "Post-buckling analysis of piezo-magnetic nanobeams with geometrical imperfection and different piezoelectric contents", *Microsyst. Technologies*, **25**(9), 3477-3488.

Mirjavadi, S.S., Forsat, M., Barati, M.R., Abdella, G.M., Afshari, B.M., Hamouda, A.M.S. and Rabby, S. (2019), "Dynamic response of metal foam FG porous cylindrical micro-shells due to moving loads with strain gradient size-dependency", *Eur. Phys. J. Plus*, **134**(5), 214.

Mori, T. and Tanaka, K. (1973), "Average stress in matrix and average elastic energy of materials with misfitting inclusions", *Acta metallurgica*, **21**(5), 571-574. https://doi.org/10.1016/0001-6160(73)90064-3.

Rahmani, M.C., Kaci, A., Bousahla, A.A., Bourada, F., Tounsi, A., Bedia, E.A. and Tounsi, A. (2020), "Influence of boundary conditions on the bending and free vibration behavior of FGM sandwich plates using a four-unknown refined integral plate theory", *Comput. Concrete*, **25**(3), 225-244. https://doi.org/10.12989/cac.2020.25.3.225.

Refrafi, S., Bousahla, A.A., Bouhadra, A., Menasria, A., Bourada, F., Tounsi, A. and Tounsi, A. (2020), "Effects of hygro-thermo-mechanical conditions on the buckling of FG sandwich plates resting on elastic foundations", *Comput. Concrete*, **25**(4), 311-325. https://doi.org/10.12989/cac.2020.25.4.311.

Safaei, B., Moradi-Dastjerdi, R., Qin, Z. and Chu, F. (2019). "Frequency-dependent forced vibration analysis of nanocomposite sandwich plate under thermo-mechanical loads", *Compos. Part B: Eng.*, **161**, 44-54.

Safarpour, M., Ghabussi, A., Ebrahimi, F., Habibi, M. and Safarpour, H. (2020), "Frequency characteristics of FG-GPLRC viscoelastic thick annular plate with the aid of GDQM", *Thin-Wall. Struct.*, **150**, 106683. https://doi.org/10.1016/j.tws.2020.106683.

Sahla, M., Saidi, H., Draiche, K., Bousahla, A.A., Bourada, F. and Tounsi, A. (2019), "Free vibration analysis of angle-ply laminated composite and soft core sandwich plates", *Steel Compos. Struct.*, **33**(5), 663. https://doi.org/10.12989/scs.2019.33.5.663.

Semmah, A., Heireche, H., Bousahla, A.A. and Tounsi, A. (2019), "Thermal buckling analysis of SWBNNT on Winkler foundation by non local FSDT", *Adv. Nano Res.*, **7**(2), 89. https://doi.org/10.12989/anr.2019.7.2.089.

Soltani, K., Bessaim, A., Houari, M.S.A., Kaci, A., Benguediab, M., Tounsi, A. and Alhodaly, M.S. (2019), "A novel hyperbolic shear deformation theory for the mechanical buckling analysis of advanced composite plates resting on elastic foundations", *Steel Compos. Struct.*, **30**(1), 13-29. https://doi.org/10.12989/scs.2019.30.1.013.

Thanh, C.L., Tran, L.V., Vu-Huu, T. and Abdel-Wahab, M. (2019), "The size-dependent thermal bending and buckling analyses of composite laminate microplate based on new modified couple stress theory and isogeometric analysis", *Comput. Method. Appl. M.*, **350**, 337-361. https://doi.org/10.1016/j.cma.2019.02.028.

Tlidji, Y., Zidour, M., Draiche, K., Safa, A., Bourada, M., Tounsi, A. and Mahmoud, S.R. (2019), "Vibration analysis of different material distributions of functionally graded microbeam", *Struct. Eng. Mech.*, **69**(6), 637-649. https://doi.org/10.12989/sem.2019.69.6.637.

Tounsi, A., Al-Dulaijan, S.U., Al-Osta, M.A., Chikh, A., Al-Zahrani, M.M., Sharif, A. and Tounsi, A. (2020), "A four variable trigonometric integral plate theory for hygro-thermo-mechanical bending analysis of AFG ceramic-metal plates resting on a two-parameter elastic foundation", *Steel Compos. Struct.*, **34**(4), 511-524. https://doi.org/10.12989/scs.2020.34.4.511.

Vinyas, M. and Kattimani, S.C. (2017), "A finite element based assessment of static behavior of multiphase magneto-electro-elastic beams under different thermal loading", *Struct. Eng. Mech.*, **62**(5), 519-535. https://doi.org/10.12989/sem.2017.62.5.519.

Vinyas, M. and Kattimani, S.C. (2017), "Static analysis of stepped functionally graded magneto-electro-elastic plates in thermal environment: a finite element study", *Compos. Struct.*, **178**, 63-86.

Vinyas, M. and Kattimani, S.C. (2017), "Hygrothermal analysis of magneto-electro-elastic plate using 3D finite element analysis", *Compos. Struct.*, **180**, 617-637.

Vinyas, M. and Kattimani, S.C. (2017), "A 3D finite element static and free vibration analysis of magneto-electro-elastic beam", *Coupled Syst. Mech.*, **6**(4), 465-485. https://doi.org/10.12989/csm.2017.6.4.465.

Vinyas, M. and Kattimani, S.C. (2018), "Investigation of the effect of BaTiO3/CoFe2O4 particle arrangement on the static response of magneto-electro-thermo-elastic plates", *Compo. Struct.*, 185, 51-64.

Vinyas, M., Sandeep, A.S., Nguyen-Thoi, T., Ebrahimi, F. and Duc, D.N. (2019), "A finite element–based assessment of free vibration behaviour of circular and annular magneto-electro-elastic plates using higher order shear deformation theory", *J. Intel. Mat. Syst. Str.*, **30**(16), 2478-2501.

Vinyas, M., Nischith, G., Loja, M.A.R., Ebrahimi, F. and Duc, N.D. (2019), "Numerical analysis of the vibration response of skew magneto-electro-elastic plates based on the higher-order shear deformation theory", *Compos. Struct*., **214**, 132-142.

Vinyas, M., Harursampath, D. and Nguyen-Thoi, T. (2019), "Influence of active constrained layer damping on the coupled vibration response of functionally graded magneto-electro-elastic plates with skewed edges", *Defence Technology*.

Vinyas, M. (2020), "Computational analysis of smart magneto-electro-elastic materials and structures: Review and classification", *Arch. Comput. Method. E.*, 1-44. https://doi.org/10.1007/s11831-020-09406-4.

Vinyas, M. (2020), "On frequency response of porous functionally graded magneto-electro-elastic circular and annular plates with different electro-magnetic conditions using HSDT", *Compos. Struct.*, **240**, 112044. https://doi.org/10.1016/j.compstruct.2020.112044.

Vinyas, M. (2020), "Interphase effect on the controlled frequency response of three-phase smart magneto-electro-elastic plates embedded with active constrained layer damping: FE study", *Mater. Res. Express*, **6**(12), 125707.

Vinyas, M., Harursampath, D. and Thoi, T.N. (2020), "A higher order coupled frequency characteristics study of smart magneto-electro-elastic composite plates with cut-outs using finite element methods", *Defence Technology*, https://doi.org/10.1016/j.dt.2020.02.009.

Vo, T.P., Thai, H.T., Nguyen, T.K., Lanc, D. and Karamanli, A. (2017), "Flexural analysis of laminated composite and sandwich beams using a four-unknown shear and normal deformation theory", *Compos. Struct.*, **176**, 388-397.

Wang, Y., Zeng, R. and Safarpour, M. (2020), "Vibration analysis of FG-GPLRC annular plate in a thermal environment", *Mech. Based Des. Struc.*, 1-19. https://doi.org/10.1080/15397734.2020.1719508.

Wattanasakulpong, N. and Chaikittiratana, A. (2015), "Exact solutions for static and dynamic analyses of carbon nanotube-reinforced composite plates with Pasternak elastic foundation", *Appl. Math. Model.*, **39**(18), 5459-5472. https://doi.org/10.1016/j.apm.2014.12.058.

Wu, H., Kitipornchai, S. and Yang, J. (2017), "Thermal buckling and postbuckling of functionally graded graphene nanocomposite plates", *Mater. Design*, **132**, 430-441. https://doi.org/10.1016/j.matdes.2017.07.025.

Zarga, D., Tounsi, A., Bousahla, A.A., Bourada, F. and Mahmoud, S.R. (2019), "Thermomechanical bending study for functionally graded sandwich plates using a simple quasi-3D shear deformation theory", *Steel Compos. Struct.*, **32**(3), 389-410. https://doi.org/10.12989/scs.2019.32.3.389.

Zaoui, F.Z., Ouinas, D. and Tounsi, A. (2019), "New 2D and quasi-3D shear deformation theories for free vibration of functionally graded plates on elastic foundations", *Compos. Part B: Eng.*, **159**, 231-247. https://doi.org/10.1016/j.compositesb.2018.09.051.

Zhang, L.W., Zhang, Y. and Liew, K.M. (2017), "Vibration analysis of quadrilateral graphene sheets subjected to an in-plane magnetic field based on nonlocal elasticity theory", *Compos. Part B: Eng.*, **118**, 96-103.

Zhao, Z., Feng, C., Wang, Y. and Yang, J. (2017), "Bending and vibration analysis of functionally graded trapezoidal nanocomposite plates reinforced with graphene nanoplatelets (GPLs)", *Compos. Struct.*, **180**, 799-808. https://doi.org/10.1016/j.compstruct.2017.08.044.

Appendix

$$S_{1111}=\frac{1}{2\left(1-\mu_m\right)}\left(\begin{array}{l}1-2\mu_m+\dfrac{3\alpha^2-1}{\alpha^2-1}\\-\left(1-2\mu_m+\dfrac{3\alpha^2}{\alpha^2-1}\right)\tilde{J}\end{array}\right) \tag{A1}$$

$$\begin{aligned}S_{2222}&=\frac{3}{8\left(1-\mu_m\right)}\frac{\alpha^2}{\alpha^2-1}\\&+\frac{1}{4\left(1-\mu_m\right)}\left(1-2\mu_m-\frac{9}{4\left(\alpha^2-1\right)}\right)\tilde{J}\end{aligned} \tag{A2}$$

$$S_{2233}=\frac{1}{4\left(1-\mu_m\right)}\left(\begin{array}{l}\dfrac{\alpha^2}{2\left(\alpha^2-1\right)}\\-\left(1-2\mu_m+\dfrac{3}{4\left(\alpha^2-1\right)}\right)\tilde{J}\end{array}\right) \tag{A3}$$

$$\begin{aligned}S_{2211}&=-\frac{1}{2\left(1-\mu_m\right)}\frac{\alpha^2}{\alpha^2-1}\\&+\frac{1}{4\left(1-\mu_m\right)}\left(\frac{3\alpha^2}{\alpha^2-1}-\left(1-2\mu_m\right)\right)\tilde{J}\end{aligned} \tag{A4}$$

$$\begin{aligned}S_{1122}&=-\frac{1}{2\left(1-\mu_m\right)}\left(1-2\mu_m+\frac{1}{\left(\alpha^2-1\right)}\right)\\&+\frac{1}{2\left(1-\mu_m\right)}\left(1-2\mu_m+\frac{3}{2\left(\alpha^2-1\right)}\right)\tilde{J}\end{aligned} \tag{A5}$$

$$S_{2323}=\frac{1}{4\left(1-\mu_m\right)}\left(\begin{array}{l}\dfrac{\alpha^2}{2\left(\alpha^2-1\right)}\\+\left(1-2\mu_m-\dfrac{3}{4\left(\alpha^2-1\right)}\right)\tilde{J}\end{array}\right) \tag{A6}$$

$$S_{1212}=\frac{1}{4\left(1-\mu_m\right)}\left(\begin{array}{l}1-2\mu_m-\dfrac{\alpha^2+1}{\left(\alpha^2-1\right)}\\-0.5\left(1-2\mu_m-\dfrac{3\left(\alpha^2+1\right)}{\left(\alpha^2-1\right)}\right)\tilde{J}\end{array}\right) \tag{A7}$$

and

$$\tilde{J}=\frac{\alpha^2\left(\alpha^2-1\right)^{0.5}-\alpha acosh(\alpha)}{\left(\alpha^2-1\right)^{1.5}} \tag{A8}$$